Control-Oriented Model for
Camless Intake Process (Part I)

M.-S. S. Ashhab, A. G. Stefanopoulou*

Mechanical and Environmental Engr. Dept.

University of California

Santa Barbara, CA 93106-5070

J. A. Cook, M. B. Levin

Ford Motor Company

Scientific Research Laboratory

PO. Box 2053, M.D. 2036, Dearborn, MI 48121

Abstract

The improvement of internal combustion engine is largely accomplished though the introduction of innovative actuators that allow optimization and control of the flow, mixing, and combustion processes. The realization of such a novel system depends on the existence of an operational controller that will stabilize the engine and allow experimental testing which, consequently, leads to further development of the actuator and the engine controller. This iterative process requires a starting point which is the development of a control-oriented model. Although not fully validated, the control-oriented model reveals issues associated with uncertainties, nonlinearities, and limitation of different subsystems. Moreover, it aides in defining the controller structure and the necessary parameters for the calibration of the closed loop system. In this paper (Part I) we describe the development process of a control-oriented model for a camless intake process.

1 Introduction

Various analytical and experimental studies of engines equipped with innovative valvetrain mechanisms have shown that controlling cylinder air charge with the intake valve motion can reduce pumping losses and thus increase fuel economy (Elrod and Nelson, 1986; Gray, 1988; Ma, 1986). This is achieved by eliminating the need to throttle the air flow into the intake manifold which is the traditional means of controlling the engine load in spark ignition engines. By using electronically controlled intake valvetrain developed in (Schechter and Levin, 1996), one can eliminate the main throttle body and directly regulate the air flow into the cylinders. We refer to this engine conditions as unthrottled operation.

An automatic controller is necessary to regulate the additional degrees of freedom of camless engine operation, namely, valve lift and opening-closing timing. Developing such a controller requires knowledge of how, at least qualitatively, the additional degrees of freedom affect the engine intake process. It is, thus necessary to develop an engine model for control development eventhough experimental data of the actual system are not available. In this paper we concentrate in capturing the dominant dynamic behavior of the intake process and investigate the sensitivity of the model to higher order dynamics that are in general uncertain or difficult to model. In contrast to the mathematical models developed for subsystem optimization, our goal is to reveal potential difficulties in the control design due to subsystem limitations, nonlinearities, and uncertainty. We first develop a phenomenological multicylinder and crankangle based model of the intake process. The crankangle based model consists of dynamical equations (using first principles and engine/actuator geometrical characteristics) and static empirical relations (based on data) and is validated against experimental data of a conventional engine with cam-driven valve profile during unthrottled operation. We then derive the control-oriented model for the cylinder air charge and the pumping losses assuming uniform air pulses during the intake duration. We show that this assumption leads to a simple input-output representation that can be used for the development of a cylinder air charge controller and for the minimization of pumping losses. We finally, investigate the modeling uncertainty due to often unknown higher order dynamics. This paper is intended to fill the gap between the work on camless actuation design, and the work related to steady-state engine optimization.

Work in the area of actuator design can be found in (Gray, 1988; Moriya et al., 1996; Schechter and Levin, 1996) and references therein. Only few papers in this category address issues associated with closed loop actuator operation and performance that enable steady-state engine operation. The most comprehensive study of the inner loop controller for a camless valvetrain actuator can be found in (Anderson et al, 1998). The authors develop and test an adaptive algorithm for maximum lift control that enables stable actuator operation for the electro-hydraulic camless valvetrain developed in (Schechter and Levin, 1996) and modeled in (Kim et al., 1997). Engine optimization studies and sensitivity analysis can be found in (Gray, 1988; Ahmad and Theobald, 1989; Sono and Umiyama, 1994; Ashhab et al., 1998). Finally, studies on the feedback controller design and the engine management system are scarce (Urata et al., 1993; Ashhab et al., 1998).

In (Urata et al., 1993) the authors tune a proportional-derivative idle speed controller. They also design an air-to-fuel ratio (A/F) feedback loop by using oxygen sensor in the exhaust of each cylinder and correct individual cylinder intake valve timing. A more attractive solution of balancing A/F maldistributions is demonstrated in (Moraal et al., 1995) where a single manifold pressure sensor is used to estimate conventional valvetrain component variability and then adjust fuel pulsewidth duration of individual cylinders. In all the previous work neither unthrottled nor camless operation was considered and the results are restricted to a 4-cylinder case.

This paper is organized as follows. We describe the crankangle-based phenomenological engine model with the camless actuator in Section 2. Section 3 includes validation results. The control-oriented model is then derived in Section 4 and in Section 5 we calculate uncertainty models for control development. It is shown that high order inertial and acoustic flow characteristics alter intake flow during unthrottled operation and increase the uncertainty of the mean-value model requiring robust or adaptive controller development.

2 Multicylinder Breathing Process

Control-oriented engine models are primarily based on mean value approximation of the engine states after averaging over an engine event (see (Powell and Cook, 1987) and references therein). The averaged representation is accurate over the frequencies of interest, which are defined by (i) the sensor and actuator bandwidths, and (ii) the event based breathing process. A camless engine allows control of the intake valve events independently from the piston motion. To develop its mean value breathing characterization, we model the crankangle-based breathing process coupled with a time-based quasi-static intake valve profile of a springless electro-hydraulic valvetrain.

2.1 Pressure Dynamics

The dynamic equations that describe the breathing process are based on the principles of the conservation of mass and the ideal gas law. Differences in intake flow temperature and manifold temperature can be neglected for the intake event. Consider the manifold pressure, p_m, and the cylinders pressures, p_{c_i}, $i = 1, \ldots n$, where the subscript i denotes the ith cylinder, and n is the number of the cylinders. Their time derivative are derived from the ideal gas law $pV = mRT$, where p is pressure (Pascal), V is volume (m^3), m is air mass (kg) trapped in the volume V, T is temperature (K), and R is the gas constant for air (J/kgK). The state equations are given as

$$\frac{dp_m}{dt} = \frac{RT}{V_m}\left[\dot{m}_\phi - \sum_{i=1}^n \dot{m}_{c_i}\right] \quad (1)$$

$$\frac{dp_{c_i}}{dt} = \frac{1}{V_{c_i}}\left[RT\dot{m}_{c_i} - \dot{V}_{c_i}p_{c_i}\right], \quad i = 1, \ldots, n, \quad (2)$$

where, $\dot{m}_\phi$ is the mass air flow through the throttle (kg/s), $\dot{m}_{c_i}$ is the mass air flow from the manifold into cylinder i (kg/s), V_m is the manifold volume (m^3), and V_{c_i} is the ith cylinder volume (m^3). The cylinder volume is a function of the crank angle (θ) in degrees:

$$V_{c_i}(\theta) = \frac{V_d}{2}\left(1 - \cos(\theta - \frac{720}{n}(i-1))\right) + V_{cl}, \quad (3)$$

$$\theta = \left(\int_0^t \frac{N}{60}360 \cdot d\tau\right) \bmod 720^o, \quad (4)$$

where, V_d is the maximum cylinder displaced volume, V_{cl} is the cylinder clearance volume, and N is the engine speed (RPM). Exact values for all engine parameters for a 4-cylinder experimental engine used for the model validation can be found in Appendix A.

The pressures in the intake manifold and cylinders are assumed to be homogeneous and spatially uniform due to the large volumes associated with the processes. On the other hand, the intake runners allow the development of standing waves forced by the piston motion when the intake valve opens. Thus, the spatial variation of pressure in the inlet runners determines the pressure at the inlet port (p_{r_i}) and consequently the flow through the intake valve into the cylinder $(\dot{m}_{c_i})$. To avoid using a spatially distributed model of the runner pressure we adapt an one-dimensional model introduced in (Broome, 1969) in describing the phenomenon of induction ram, and later in (Ohata and Ishida, 1982; Moraal et al., 1995) in calculating in-cylinder flow. Specifically, the pressure drop in each inlet port is a function of the spatially distributed gas velocity, $v_{g_i}(x,t)$, evaluated at the inlet port x_r:

$$p_{r_i} = p_m - \Delta p_{r_i} \quad (5)$$

$$\Delta p_{r_i} = m_r \frac{k_r}{A_r}\frac{dv_{g_i}(x_r,t)}{dt}. \quad (6)$$

where, m_r is the averaged runner mass, $m_r = \frac{p_m V_r}{RT}$, V_r is the runner volume (m^3), A_r is the runner cross sectional area (m^2), k_r is a calibration constant that depends on the geometry of the runners (see Appendix A).

Let us for simplicity define the time dependent gas velocity of the inlet port, $v_{g_i}(x_r,t) \doteq v_{r_i}$. The inlet port gas velocity, v_{r_i}, can be approximated (Broome, 1969; Moraal et al., 1995) by the solution to a second order forced differential equation with known initial values:

$$A_r\left(\frac{1}{\omega_h^2}\frac{d^2}{dt^2}v_{r_i} + 2\xi_h\frac{1}{\omega_h}\frac{d}{dt}v_{r_i} + v_{r_i}\right) = \frac{\pi B^2}{4}v_{p_i} \quad (7)$$

$$\text{with} \quad \begin{aligned} v_{r_i}(t = t_{IVO_i}) &= 0 \\ \frac{d}{dt}v_{r_i}(t = t_{IVO_i}) &= 0. \end{aligned} \quad (8)$$

The forcing function of Eq. 7 depends on the piston cross sectional area $\frac{\pi B^2}{4}$, (m^2), and the the piston velocity, $v_{p_i} = \frac{2\pi N}{120}S\sin\left(\theta - \frac{720}{n}(i-1)\right)$, (m/s). The constants

B and S are the cylinder bore (m) and stroke (m), respectively. Exact values of these parameters are given in Appendix A. The initial conditions (Eq. 8) are based on the fact that the inlet port gas velocity and acceleration are zero when the intake valve opens. It is important to note here that Eq. 7 is evaluated for each cylinder in time domain starting when the intake valve opens and terminates when the intake valve closes. The gas velocity at the port is a damped oscillation based on a Helmholtz resonator equivalent model, where ω_h is the natural frequency and ξ_h is the damping ratio. Both ω_h and ξ_h can be identified using engine data.

2.2 Mass Air Flow

A quasi-steady model of flow through an orifice is used to derive the mass air flow through the throttle body and the intake valve. The quasi-steady relation of the air flow through a restriction is based on the assumptions of one-dimensional, steady, compressible flow of an ideal gas (Novak, 1977; Heywood, 1988).

$$\dot{m} = A_o d_o(p_1, p_2, T_1, T_2), \qquad (9)$$

where, A_o is the effective flow area of the orifice which is determined by regressing the steady-state experimental data; d_o is the standard orifice flow function that depends on the downstream pressure and temperature, p_1 and T_1, and upstream pressure and temperature, p_2 and T_2:

$$d_o(p_1, p_2, T_1, T_2) = \begin{cases} \frac{p_2}{\sqrt{RT_2}} \Psi_o\left(\frac{p_1}{p_2}\right) & \text{if } p_1 \le p_2 \\ \frac{p_1}{\sqrt{RT_1}} \Psi_o\left(\frac{p_2}{p_1}\right) & \text{if } p_1 > p_2, \end{cases} \quad (10)$$

with

$$\Psi_o(x) = \begin{cases} \gamma^{\frac{1}{2}} \left(\frac{2}{\gamma+1}\right)^{\frac{\gamma+1}{2(\gamma-1)}} & \text{if } x \le r_c \\ x^{\frac{1}{\gamma}} \sqrt{\frac{2\gamma}{\gamma-1}\left(1 - x^{\frac{\gamma-1}{\gamma}}\right)} & \text{if } x > r_c, \end{cases} \quad (11)$$

where, $r_c = \left(\frac{2}{\gamma+1}\right)^{\frac{\gamma}{\gamma-1}}$ is the critical pressure ratio.

The above expression is simplified by taking into account that for camless unthrottled operation the intake manifold pressure is almost equal to the ambient pressure $p_o = 10^5$ Pa. In addition we consider $T_1 = T_2 = T = 316^o$ K, $R = 287$ J/kgK, γ=1.4 and that typical operation results in limited backflow through the orifice ($p_1/p_2 \le 1.1$). Thus, the flow through the throttle body, $\dot{m}_\phi$, and the intake valve, $\dot{m}_{c_i}$, are written as

$$\dot{m}_\phi = A_\phi(\phi) d(p_m, p_o) \quad \text{and} \qquad (12)$$
$$\dot{m}_{c_i} = A_{v_i}(L_{v_i}) d(p_{c_i}, p_m), \qquad (13)$$

respectively, where, $p_o = 1$ bar denotes the ambient pressure, A_ϕ is the effective throttle body area (m^2) as a function of throttle position, ϕ (defined in Appendix A). Note here that $\phi = 90^o$ during unthrottled operation. Also, A_{v_i} is the valve effective area (m^2) defined in the next section, and L_{v_i} is the intake valve lift (mm).

2.3 Intake Valve Profile and Effective Flow Area

Variable valve motion is achieved by continuously varying the valve timing (or opening), IVO, maximum lift, IVL, and duration, IVD, using an experimental springless electro-hydraulic valvetrain developed by (Schechter and Levin, 1996). This valvetrain exploits the principle of the hydraulic pendulum concept to achieve high energy recovery during the opening and closing of the engine valves by converting the potential energy of the high pressure fluid to kinetic energy of the moving valve and vice-versa. A detailed dynamic model of the electro-hydraulic can be found in (Kim et al., 1997). The opening, maximum lift, and closing of the valves is controlled by solenoid valves that regulate high pressure fluid in various control chambers of the actuator. A high bandwidth controller is necessary to regulate the valve position to the desired profile. We call this controller the "inner loop controller" (Anderson et al, 1998). In this work we will assume the existence and stability of the inner loop.

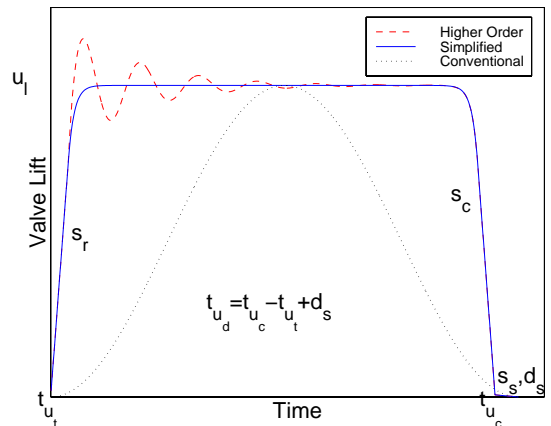The valve profiles are shown in Figure 1. The solid-line

Figure 1: Electro-hydraulic camless (dashed), simplified camless (solid), and conventional (dotted) intake valve profiles.

shows the desired valve position as generated through the outer loop controller and the dashed line is the closed loop valve behavior. Note that the closed loop valve behavior, shown with dashed line, exhibits a decaying oscillations at the end of the acceleration stage. This oscillatory behavior is the result of low system damping that is required to maintain the high levels of energy recovery of the valvetrain. For the purpose of developing a mean value model for engine control development it is important to quantify the importance of the high frequency component of the actuator dynamics. In a later section we investigate the effect of these dynamics on the mean value model. The conventional valve profile is also plotted with dotted line in Figure 1 for comparison.

We parameterize the motion by the slope of the opening, s_r, slope of the closing, s_c, slope and duration of

3

the seating, s_s and d_s, and λ which determines how fast the valve motion approaches the maximum lift after the opening. To simplify the notation and because timing (or opening), IVO, maximum lift, IVL, and duration, IVD, of each intake valve will be in the sequel controlled electronically, we define them as u_t, u_l and u_d respectively. There are two sets of equations describing the valve motion, $\tilde{L}_v = \tilde{L}_v(u_t, u_l, u_d, t)$, and the simplified (non-oscillatory) valve motion, $L_v = L_v(u_t, u_l, u_d, t)$. The profile is shaped using fixed in time domain constants s_r, s_c, s_s, and d_s. Thus, a coordinate transformation to crank angle domain results in different valve profiles for different engine speeds as shown in Figure 2.
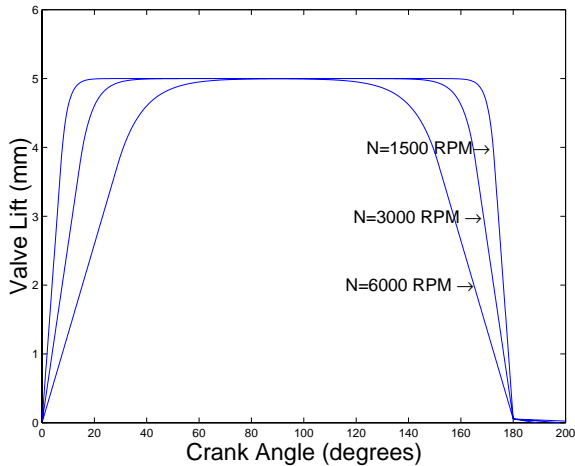

Figure 2: Intake valve profiles for different speeds.

The scaled effective flow area can be determined using experimental flowbench data from the camless prototype system. Although these accurate measurements are currently not available, we can approximate the scaled effective valve flow area with a linear function of the lift

$$A_v(L_v) = \alpha L_v. \tag{14}$$

The scalar α can be identified by using engine data from a cam-driven valvetrain system with a sinusoidal profile. The electro-hydraulically driven valve opens very fast thus the uncertainty with respect to the low lift areas is minimized. In Section 3 we use $\alpha = 0.0175$ for an experimental 4 cylinder engine. The validation results in Section 3 suggest that the approximation is adequate for control design purpose since steady-state errors will be adjusted using feedback.

2.4 Cylinder Air Charge

The cylinder air charge is the total air mass trapped in the cylinder during the induction process:

$$m = \int_{t_{IVO}}^{t_{IVO}+t_{IVD}} \dot{m}_c dt.$$

The simulation results are shown in Figure 3 for a 4– cylinder engine at an engine speed of 1500 RPM. The model described in the previous section was coded in Matlab Simulink CACSD software. The model does not take into account the overlap between the intake and exhaust valves[1] and describes only the intake event of the engine cycle. Therefore, we assume that the cylinder pressure when the intake valve opens, $p_{c_i}(IVO_i)$, is equal to the cylinder pressure at the end of the exhaust stroke. In turn, we assume that the cylinder pressure at the end of the exhaust stroke is equal to the exhaust backpressure, $p_{c_i}(IVO_i) = p_{c_i}(EVC_i) = 1.1$ bar. Thus, each cylinder pressure is initialized at the beginning of every intake event by triggering the cylinder pressure integrator in the simulation model.

The simplified intake valve motion is plotted in subplot 1. The intake valve opening (IVO) is equal to 0° ATDC, lift is equal to 3 mm, and closing timing is equal to 180°. Note that the intake valve duration IVD is equal to the closing timing plus the seating duration. In this case, $IVD = 189^o$. The corresponding manifold, and cylinder pressures are plotted in subplot 2. The manifold pressure stays close to the atmospheric pressure due to the unthrottled operation. Subplot 3 shows the mass air flows through the throttle and intake port, which are very similar because the rate of change of the manifold pressure is small (see Eq. (1)). Note the backflow at the beginning of the induction stroke which occurs due to the high cylinder pressure. The mass air flow across the intake port stops after the intake valve closes. However, the mass air flow through the throttle is not equal to zero since the following cylinder intake valve is open. The resulting cylinder air charge in Figure 3 is equal to $4.73 \cdot 10^{-4}$ kg/event.

2.5 Pumping Loses

The pumping loss, E, is the area enclosed by the loop formed by the cylinder pressure below the exhaust manifold pressure when plotted versus piston displacement. Specific pumping loss defined as the ratio of pumping losses over cylinder air charge, e, is considered as a measure of fuel economy:

$$E = \int_{t_{IVO}}^{t^*} (p_{exh}(t) - p_c(t))dt, \text{ and } e = E/m,$$

where, p_{exh} is the exhaust pressure. We assume that the cylinder pressure is equal to the exhaust pressure for the majority of the exhaust stroke, $p_{c_i}(EVC_i) = 1.1$ bar.

Having defined the pumping losses in the simulation model allows us to demonstrate one of the advantages of the camless engine over the conventional engine. Namely, unthrottled operation results in low pumping loss when

---

[1] To avoid future confusion, we call "valve overlap" the overlap between the exhaust and the intake valve of the same cylinder. Accordingly, we call "cylinder overlap" the intake valve overlap of different cylinders.
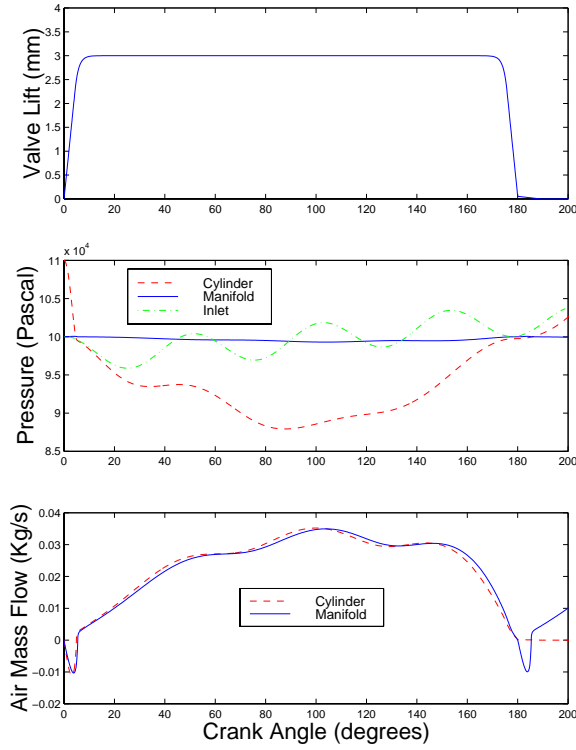
Figure 3: Engine breathing characteristics of a 4-cylinder engine at an engine speed of 1500 RPM.

compared to a conventional engine operation at the same load. Specifically, for a valve lift of 2 mm and duration of 99° (early closing) at an engine speed of 1500 RPM, the corresponding cylinder air charge is equal to $1.71 \cdot 10^{-4}$ kg. The conventional engine with a throttle angle $\phi = 17^o$ produces the same load at the same speed. The corresponding negative work loop of the $P - V$ diagrams of the camless and conventional engines are shown in Figure 4. The short intake valve duration results in a reversible isothermal process after the intake valve closes. The calculated pumping losses are 3.55 J and 13.8 J for the camless and conventional engines, respectively. Thus, unthrottled engine operation using camless valvetrain results in 74% reduction in pumping losses which agrees with results presented in (Miller et al., 1997) for the above-mentioned load.

3   Validation

The model described in this paper was evaluated using experimental data for a 4-cylinder engine (Moraal et al., 1995) during wide open throttle operation. The valves of the experimental engine are cam-driven, therefore, the intake valve profile is the conventional sinusoidal profile with the following specifications: (i) intake valve opening: 8° BTDC, (ii) intake valve closing: 46° ABDC, (iii) maximum valve lift: 8.1 mm, resulting in the intake profile for
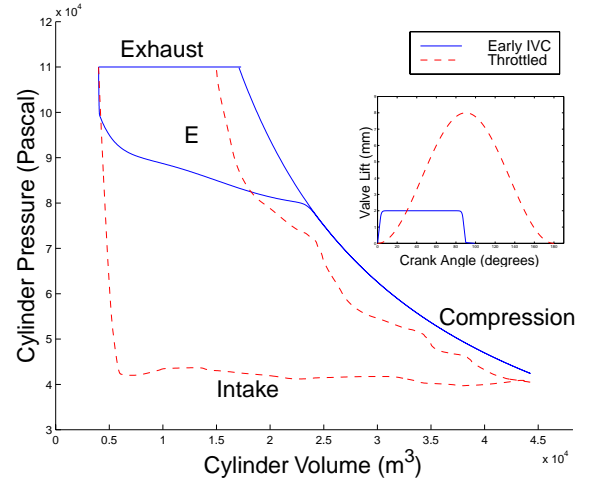

Figure 4: Cylinder $P - V$ diagrams that demonstrate the pumping loss in a throttled and a camless unthrottled engine (lift profiles are also shown).

cylinder No. 1:

$$L_v\left(u_t, u_l, u_d, \theta\right) = u_l \cdot \sin^2\left(\frac{180}{u_d}(\theta - u_t)\right),$$

with $u_l = 8.1$ mm, $u_d = 234^o$, and $u_t = -8^o$. The term θ is as in Equation (4). The valve effective area is given in Eq. 14 with $\alpha = 0.0175$. Geometric specifications are the same as those used for the model and are given in Appendix A.

In Figures 5, and 6 we compare the model with the actual engine data for wide open throttle (ϕ in Equation (12) is fixed to 90°) and engine speeds of 1500, and 3000, respectively. The manifold and cylinder pressures are plotted for the model (dashed curve) and the experimental engine (solid curve). The model Helmholtz resonator parameters were determined as $w_h = 2\pi * 176$, $\xi_h = 0.005$ for an engine speed of 1500 RPM, and $w_h = 2\pi * 190$, $\xi_h = 0.15$ for engine speed of 3000 RPM. These values are similar to the ones identified in (Moraal et al., 1995).

Note that the model captures most of the dynamic effects. Moreover, the model predicts rather accurately the integral quantities, namely, the cylinder air charge and pumping losses, which are overall measures of the engine performance over the induction stroke. The comparison of predicted cylinder air charge ($\hat{m}$) and pumping loss ($\hat{E}$) versus the actual data cylinder air charge (m) and the pumping loss (E) follows:

N	$\hat{m}$	m	$\hat{E}$	E
1500	477.4	506.9	5.2	5.7
3500	503.3	545.6	8.9	7.9

The maximum error in air charge prediction can be calculated to be less that 10% and the maximum error in pumping losses is 11.3%. Note also, that the model captures the 18° overlap between the intake and exhaust valves.
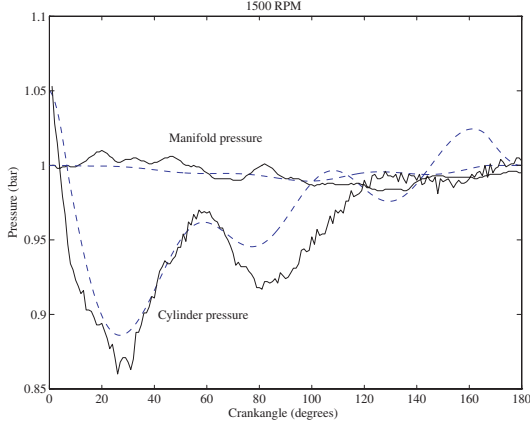
Figure 5: Model comparison at 1500 RPM. The model predicted manifold and cylinder pressures are plotted with the dashed linetype whereas the experimental traces are shown with the solid linetype.
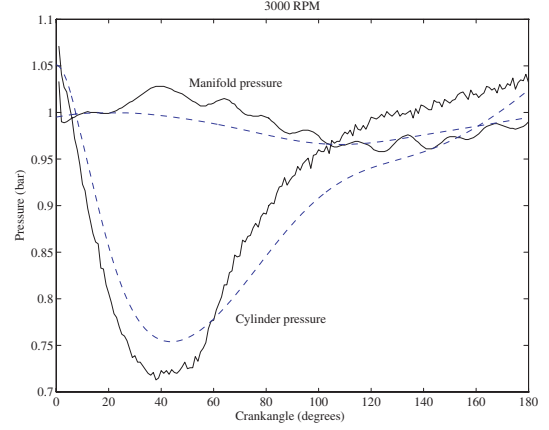

Figure 6: Model comparison at 3000 RPM. The model manifold and cylinder pressures are shown with in dashed linetype whereas the actual pressure traces are shown with the solid linetype.

4 Control-Oriented Model

To facilitate the control development of a variable intake valve timing engine we derive a mean-value model of the variable valve breathing process using the previously developed crankangle-domain model. Specifically, we assume cylinder-to-cylinder balanced uniform pulse homogeneous charge, that allows us to model the cylinder air charge (mass air trapped into the cylinders per event, kg/event) and the pumping losses (J/event) in continuous time-domain as functions of the maximum lift, u_l, and duration, u_d.

The input-output behavior is derived for fixed intake valve timing, u_t, and parametrically varying intake valve maximum lift, u_l, and duration, u_d in the crankangle-domain model . We fix u_t to zero degrees ATDC, because neither advancing nor retarding u_t affects the performance variables in a favorable way (Ashhab et al., 1998). This result is in agreement with the work of Miller et al. in (Miller et al., 1997) where u_t was set to zero at all loads and medium engine speed. Note, that by setting $u_t = 0$ degrees $ATDC$, valve closing is approximately equal to the valve duration. The input-output mean-value model can now be described by a static nonlinearity that is identified by fitting data attained by simulation, and a delay:

$$\begin{aligned} m(t + \Delta T) &= F_m^o(u_l(t), u_d(t), N(t)) \\ e(t + \Delta T) &= F_e^o(u_l(t), u_d(t), N(t)), \end{aligned} \quad (15)$$

here u_l and u_d are the lift and duration commands to the camless actuator, N is the engine speed, and ΔT is the compression-to-power delay. The static maps F_m^o and F_e^o for engine speed equal to 1500 RPM are shown in Figures 7 and 8. It is important here to qualitatively compare the unthrottled camless cylinder air charge with the typical conventional cylinder air charge representation:

$$m(t + \Delta T) = F_m^{conv}(p_m(t), N(t)),$$

where p_m is the intake manifold pressure. Note, here that the mean-value camless cylinder air charge does not depend on manifold pressure because of the unthrottled conditions.
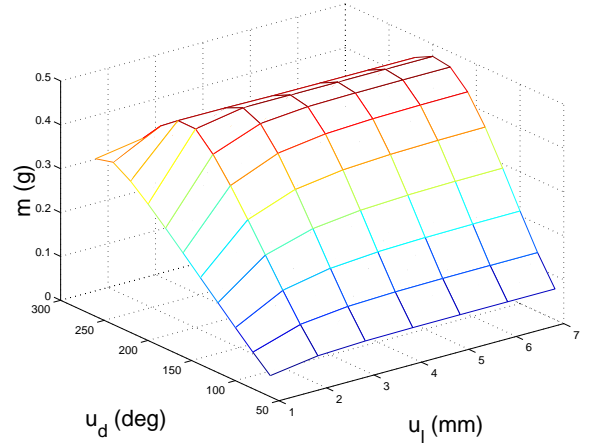

Figure 7: Mean-value cylinder air charge.

The cylinder air charge is an increasing – almost linear – function of the intake valve lift for intake valve lifts less than 3 mm. The trapped cylinder air charge does not increase appreciably above 3 mm of lift. This occurs because the inlet and cylinder pressures become almost equal for most of the induction process which reduces the rate of mass air flow between the cylinder and the runners. The region where cylinder air charge becomes insensitive to u_l we call "lift saturation region." The lift saturation region occurs in higher levels of lift for higher speeds and vice-versa for lower engine speeds (ex. lift saturates at 5 mm for 5500 RPM, and at 1.5 mm for 750 RPM). The pumping loss behaves in a similar way. The specific pumping loss
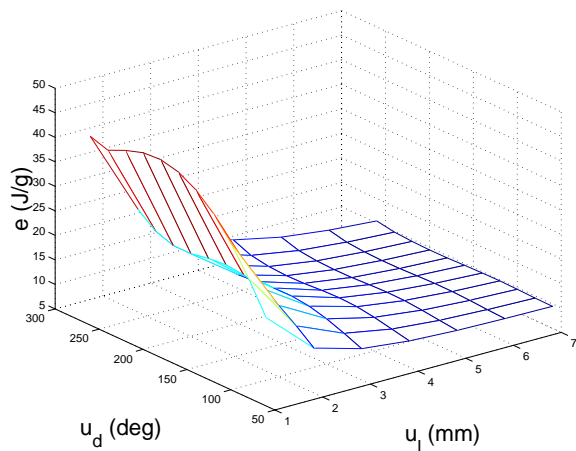
Figure 8: Mean-value pumping losses.

is a decreasing function of the intake valve lift since larger lifts allow the cylinder to be more efficient in pumping air from the manifold.

The cylinder air charge is a monotonically increasing function of the intake valve duration for $u_d \leq 180$. For larger valve duration, $u_d > 180$, cylinder air charge decreases due to the backwards flow from the cylinder to the manifold, which occurs during the upward motion of the piston. We call this region as "flow reversal region." The flow reversal region occurs at higher values of valve duration for faster speeds. At high engine speeds the valve opening rate is small (see rising slope in Figure 2), thus, requiring longer valve durations than the intake event. Thus, it is obvious that to achieve high loads at high speeds the engine controller should require valve duration larger than 180°, causing significant cylinder-to-cylinder breathing overlap.

5   High Order Model Dynamics

It is important from a control perspective to investigate the effects of higher order dynamics to the mean-value model developed. In this section, we consider simplifications, firstly, in the inlet runners and, secondly, the oscillatory behavior of the actuator dynamics.

In the crank angle model development the acoustic and inertial characteristics of the mass air flow through the inlet pipes were considered. These higher order dynamics depend on the specific geometric characteristics (length, diameter, etc.) of the inlet runners that are usually defined in a later stage of the vehicle development cycle. Thus, neglecting these dynamics will be very desirable because it would allow the development of the controller even before the vehicle design is finalized. Having the controller structure and initial parameters identified early on in the vehicle development cycle can potentially reduce the time-to-market delay for a novel system.

Also, it is desirable to neglect the oscillatory behavior of the closed loop camless valve actuator. The peak and

period of the oscillation are complicated functions of the actuator hydraulic parameters and will significantly increase the complexity of the controller development if included in the engine model. Quantifying the uncertainty of the mean value model due to these higher order dynamics can assess potential errors if the inner actuator controller loop and the outer engine management control loop have to be treated independently.

5.1   Helmholtz Resonator Dynamics

In this section we neglect the spatial variation of pressure in the inlet runners. Specifically, we assume that the pressure in the inlet port, p_{r_i}, is equal to the intake manifold pressure, p_m: $p_{r_i} = p_m$. Simulation without the Helmholtz resonator dynamics eliminates the high frequency oscillations shown in the pressures and the mass air flow in Figure 3. Neglecting the Helmholtz resonator dynamics results in $2n$ less states in the model (n is the number of cylinders). Investigation of the effects of the Helmholtz dynamics to the mean-value breathing model shows that at engine speed of 1500 RPM there is a small discrepancy between the two distinct models. This is not the case, however for higher speeds. Figure 9 shows the
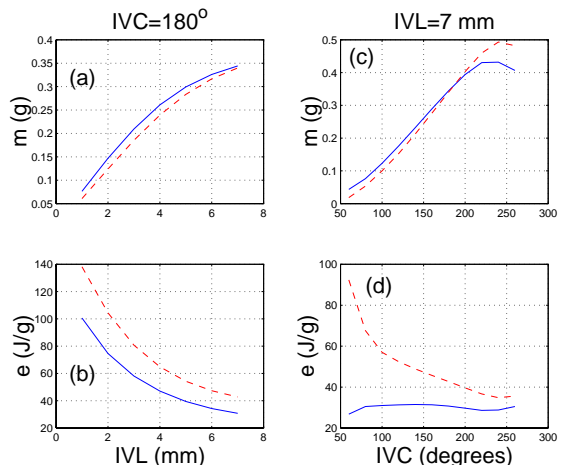

Figure 9: Investigation of the effects of the higher order inertial and acoustic dynamics to the mean-value model at an engine speed of 6000 RPM.

discrepancy between the two models for 6000 RPM. At high engine speed, Helmoltz resonator dynamics increase the cylinder air charge during late intake valve closing (ram effect as in (Broome, 1969)). This is achieved with no adverse effect in specific pumping losses. For early valve closing, however, helmholtz resonator dynamics reduce the cylinder air charge and increase the pumping losses. It is, thus, evident that higher order dynamics in the intake runners introduce considerable uncertainty in the mean-value model representation and have to be considered in the controller development.

This phenomenon is well known in the thermodynamic community, and in fact, it is currently used to optimize

engine volumetric efficiency at high speeds. On the other hand, it is largely neglected in the engine controller development because current emissions and fuel economy regulations correspond to low-to-medium loads and speeds. At these operating conditions conventional engines are throttled and the effects of the higher order dynamics are negligible. This cannot be the case, though, for stricter emission regulations or new engine concepts such as camless and direct injection that require unthrottled operation.

5.2 Actuator Dynamics

The oscillations at the end of the acceleration stage of the valve shown in Figure 1 is a result of the low damped highly efficient hydraulic actuator as described in (Kim et al., 1997). Using the oscillatory model of the valve profile motion $\tilde{L}_v(t) = \tilde{L}_v(u_t, u_l, u_d, t)$, with $u_t = 0$, we calculated and compared the performance variables for the two models. Simulations performed, but not included due to space limitations, demonstrate that there are small variations between the mean-value characteristics of the cylinder air charge and pumping losses with and without the higher order hydraulic actuator dynamics. The performance variables for the two models deviate a little more for higher engine speeds. At high engine speeds the intake valve remains open at maximum lift for a short period in crankangle domain. Therefore, the higher order oscillations that do not depend on speed cause more, but still not significant, distortion to the valve profile at higher engine speeds. Due to the small changes, we can conclude that the mean-value model using the overdamped simplified valve motion is adequate for cylinder air charge controller development.

6 Conclusions

A continuous in time-domain model and a mean-value model of the induction process during unthrottled camless operation were developed. The models can be used for control analysis and design to address torque response and fuel economy based on the cylinder air charge and pumping losses. Future work will expand the model and to incorporate additional engine performances closely associated with the exhaust stroke (residual gas fraction, air-to-fuel ratio, etc.). This work will lead to controller development for the camless engine breathing process.

7 Acknowledgments

The authors would like to acknowledge helpful discussions with Barry Powell, Mo Haghgooie, and Nizar Trigui from Ford Motor Co.

A Breathing Characteristics

The parameters used in Sections 2.1 are given here. The manifold volume, $V_m = 0.001$ m^3, runner cross sectional area, $Ar = 1.43 \times 10^{-4}$ m^2, runner volume, $Vr = 5 \times 10^{-4}$ m^3, cylinder displaced volume, $V_d = 4 \times 10^{-4}$ m^3,

cylinder clearance volume, $V_{cl} = 4 \times 10^{-5}$ m^3, cylinder bore, $B = 0.0806$ m, stroke, $S = 0.088$ m, ambient pressure, $p_0 = 1$ bar, and $k_r = 1.288$.

The effective throttle body area is given as

$$A_\phi = 1.268 \times 10^{-4} \left(-0.2215 - 2.275\phi + 0.23\phi^2\right).$$
(16)

References

Ahmad T. and Theobald M. A., "A Survey of Variable Valve Actuation Technology," SAE Paper No. 891674.

Anderson M., Tsao T.-C. , and Levin M., "Adaptive Lift Control for a Camless Electrohydraulic Valvetrain," SAE Paper No. 981029.

Ashhab M. S., Stefanopoulou A. G., Cook J. A., and Levin M., "Camless Engine Cotrol for Robust Unthrottled Operation," SAE Paper No. 981031.

Broome D., "Induction Ram: Part I, II, III," Automobile Engineer, April, May, June, 1969.

Elrod A. C. and Nelson M. T., 1986, "Development of a Variable Valve Timing Engine to Eliminate the Pumping Losses Associated with Throttled Operation," SAE Paper No. 860537.

Gray C., 1988, "A Review of Variable Engine Valve Timing," SAE Paper No. 880386.

Heywood J. B., *Internal Combustion Engine Fundamentals*, McGraw-Hill, 1988.

Kim D., Anderson M, Tsao T.-C., and Levin M., " A Dynamic Model of a Springless Electrohydraulic Camless Valvetrain System," SAE Paper, No. 970248.

Ma T. H., 1986, "Recent Advances in Variable Valve Timing," *Alternative and Advanced Automotive Engines*, Plenum Press, 1996.

Miller R. H., Davis G. C., Newman C. E., and Levin M. B., "Unthrottled Camless Valvetrain Strategy for Spark-Ignited Engines," Proc. ASME ICE-Vol. 29-1, pg.81-94, 1997.

Moraal P. E., Cook J. A., and Grizzle J. W., "Modeling the induction process of an automobile engine," *Control problems in industry*, I. Lasiecka and B. Morton, Ed., Birkhauser, pp. 253-270, 1995.

Moriya Y., Watanabe A., Uda H., Kawamura H., Yoshioka M., and Adachi M., "A Newly Developed Intelligent Valve Timing System - Continuously Controlled Cam Phasing as Applied to A New 3 Liter Inline 6 Engine," SAE Paper No. 960579.

Novak J. M., "Simulation of the Breathing Process and Air-Fuel Ratio Distribution Characteristics of Three-Valve, Stratified Charge Engines," SAE Paper No. 770881, 1977.

Ohata A. and Ishida Y., "Dynamic Inlet Pressure and Volumetric Efficiency of Four Cylinder Engine," SAE Paper No. 820407, 1982.

Powell B. K. and Cook J. A., "Nonlinear Low Frequency Phenomenological Engine Modeling and Analysis," Proc. 1987 Amer. Contr. Conf., Vol. 1, pp. 332-340, June 1987.

Schecter M. M. and Levin M. B., "Camless Engine," SAE Paper No. 960581, 1996.

Sono H. and Umiyama H., "A Study of Combustion Stability of Non-Throttling SI Engine with Early Intake Valve Closing Mechanism," SAE Paper No. 945009.

Urata Y., Umiyama H., Shimizu K., Fujiyoshi Y., Sono H., and Fukuo K., "A Study of Vehicle Equipped with Non-Throttling SI Engine with Early Intake Valve Closing," SAE Paper No. 930820.